Inorg. Chem. **2002**, *41*, 6824–6830

Cyclic Tetramers Composed of Rhodium(III), Iridium(III), or Ruthenium(II) Half-Sandwich and 6-Purinethiones

Kazuaki Yamanari,*,† Rie Ito,† Shiori Yamamoto,† Takumi Konno,† Akira Fuyuhiro,† Kousuke Fujioka,‡ and Ryuichi Arakawa‡

Department of Chemistry, Graduate School of Science, Osaka University, 1-16 Machikaneyama-cho, Toyonaka, Osaka 560-0043, Japan, and Department of Applied Chemistry, Kansai University, 3-3-35 Yamate-cho, Suita, Osaka 564-8680, Japan

Received July 12, 2002

Six new cyclic tetranuclear complexes $[\{M(Cp^*)(L)\}_4]^{4+}$ and $[\{Ru^{II}(L)(cymene)\}_4]^{4+}$ [$Cp^* = \eta^5$-C_5Me_5, cymene = η^6-*p*-$MeC_6H_4Pr^i$; M = Rh^{III} and Ir^{III}; HL = 6-purinethione (H_2put) and 2-amino-6-purinethione (H_2aput)] were prepared in a self-assembly manner and characterized by NMR spectroscopy, electrospray ionization mass spectrometry, and X-ray crystal structure analysis. The two crystal structures of $[\{Rh(Cp^*)(H_{0.5}put)\}_4](CF_3SO_3)_2$ and $[\{Ir(Cp^*)(Haput)\}_4](CF_3SO_3)_4$ revealed that they have similar S_4 structures with an alternate chirality array of *CACA*, and all ligands adopt a μ-1κN^9:2$\kappa^2 S^6$,N^7 coordination mode. The orientations of the four bridging ligands are alternately up and down, and they form a central square cavity. Interestingly, the cationic tetramers of the former are stacked up along the *c* axis, resulting in an infinite channel-like cavity. The driving force of this stacking is due to intermolecular double hydrogen bonds [N(1)–H···N(21) = 2.752(4) Å] at both sides of the cavity. In the two Rh^{III}- and Ru^{II}-H_2aput systems, it turned out that the dimeric species are dominantly formed in the reaction solutions but finally convert into the tetrameric species.

Introduction

6-Purinethione (H_2put) and 2-amino-6-purinethione (H_2aput) are congeners of adenine (Hade).[1] These ligands have multiple binding sites such as N(1), N(3), S^6 (or N^6H_2), N(7), and N(9). Recently our studies showed that the S^6/N(7) chelating mode is prior to the other modes as found in $[Co(put\ or\ Hput)(en)_2]^{n+}$ (en = ethane-1,2-diamine)[2] and $[Ru(H_2put)(bipy)]^{2+}$ (bipy = 2,2′-bipyridine).[3] This S^6/N(7) coordination mode still has the binding sites at N(1), N(3), and/or N(9). The potentiality has been realized in the synthesis of cyclic polynuclear complexes of $[\{Co(Hput)(tacn)\}_n]^{n+}$ (n = 3 and 4) $[\{Co(Haput)(tacn)\}_4]^{4+}$ (tacn = 1,4,7-triazacyclononane) where μ-1κN^9:2$\kappa^2 S^6$,N^7 coordination modes are found in all cases.[4] The situation is quite analogous to that of Hade. Two crystal structures of $[\{Ru(ade)(cymene)\}_4](CF_3SO_3)_4$ (cymene = η^6-*p*-$MeC_6H_4Pr^i$)[5] and $[\{Ir(Cp^*)(ade)\}_4](CF_3SO_3)_4$ ($Cp^* = \eta^5$-C_5Me_5)[6] have been reported so far, and a similar μ-1κN^9:2$\kappa^2 N^6$,N^7 coordination mode has been found there.

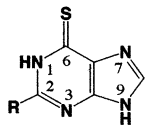

R = H H_2put
R = NH_2 H_2aput

Here we will report a synthesis of cyclic polynuclear complexes between $[M(Cp^*)(H_2O)_3]^{2+}$ (M = Rh^{III} and Ir^{III}) or $[Ru^{II}(cymene)(H_2O)_3]^{2+}$ and purinethione ligands. The

* Author to whom correspondence should be addressed. E-mail: yamanari@ch.wani.osaka-u.ac.jp.
† Osaka University.
‡ Kansai University.

(1) (a) Izatt, R. M.; Christensen, J. J.; Rytting, J. H. *Chem. Rev.* **1971**, *71*, 439−481. (b) Hodgson, D. J. *Prog. Inorg. Chem.* **1977**, *23*, 211−254.
(2) Yamanari, K.; Kida, M.; Yamamoto, M.; Fujihara, T.; Fuyuhiro, A.; Kaizaki, S. *J. Chem. Soc., Dalton Trans.* **1996**, 305−309.
(3) Yamanari, K.; Nozaki, T.; Fuyuhiro, A.; Kaizaki, S. *Bull. Chem. Soc. Jpn.* **2002**, *75*, 109−110.
(4) Yamanari, K.; Fukuda, I.; Kawamoto, T.; Kushi, Y.; Fuyuhiro, A.; Kubota, N.; Fukuo, T.; Arakawa, R. *Inorg. Chem.* **1998**, *37*, 5611−5618.
(5) Korn, S.; Sheldrick, W. S. *Inorg. Chim. Acta* **1997**, *254*, 85−91.
(6) Annen, P.; Schildberg, S.; Sheldrick, W. S. *Inorg. Chim. Acta* **2000**, *307*, 115−124.

10.1021/ic020449o CCC: $22.00
Published on Web 11/19/2002

desired complexes will be characterized by NMR spectroscopy, electrospray ionization (ESI) mass spectrometry, and X-ray crystal structure analysis. It should be noted that these systems have two different characteristics as compared with the previously reported system $[Co(tacn)(H_2O)_3]^{3+}$.[4] First, the former three metal systems are more labile than the Co^{III} system.[6,7] Hence, the solution equilibrium will be realized in the former, and the most stable complex will be formed preferentially. Second, the supporting ligands such as Cp* and cymene are expected not to participate in intraligand interactions, whereas tacn made an important contribution to the stability of the cyclic complex via intraligand hydrogen bonds in the Co^{III} system.[4] These comparisons will be discussed here.

Experimental Section

Preparations of Complexes. [{Rh(Cp*)(Hput)}$_4$](CF$_3$SO$_3$)$_4$ (1a and 1b). To a suspension of [{Rh(Cp*)Cl$_2$}$_2$][8] (0.2 g, 0.32 mmol) in water (30 cm^3) was added silver triflate (0.33 g, 1.3 mmol), and the mixture was stirred at 40 °C for 1 h. The resulting precipitate of silver chloride was removed by filtration, and to the filtrate was added an aqueous solution (50 cm^3) of H_2put (0.097 g, 0.64 mmol) adjusted to ca. pH 7 by adding aqueous NaOH. The mixed solution was stirred at room temperature for 1 day, and then the resulting solution was evaporated to give orange powder **1a**. The yield was 70−85%. Anal. Calcd for [{Rh(Cp*)(Hput)}$_4$](CF$_3$SO$_3$)$_4$·2H$_2$O **1a** ($C_{64}H_{76}F_{12}N_{16}O_{14}Rh_4S_8$): C, 35.11; H, 3.50, N, 10.24. Found: C, 35.17; H, 3.68; N, 10.51. UV−vis (water) λ_{max}, nm (ϵ, dm^3 mol^{-1} cm^{-1}): 379 sh (19 400), 330 (51 300), 265 sh (ca. 48 000), 239 (105 000). NMR (600 MHz, DMSO-d_6, 25 °C, TMS): δ_C = 166.16 (C6), 151.50 (C8 and C4), 148.41 (C2), 137.33 (C5), 95.92 (Cp*), 9.14 (Cp*). ESI MS (*m*/*z* in CH$_3$CN): 519.1 ([4M − 4X − H]$^{3+}$), 777.8 ([4M − 4X − 2H]$^{2+}$), 852.7 ([4M − 3X − H]$^{2+}$), 927.3 ([4M − 2X]$^{2+}$). The crystals [{Rh(Cp*)(H$_{0.5}$put)}$_4$](CF$_3$SO$_3$)$_2$·2Et$_2$O·6H$_2$O (**1b**) for X-ray crystal structure analysis were obtained from a DMF/ether solution of **1a**. The complex **1b** was produced from **1a** by spontaneous deprotonation during the recrystallization process.

[{Ir(Cp*)(Hput)}$_4$](CF$_3$SO$_3$)$_4$ (2). To a suspension of [{Ir(Cp*)Cl$_2$}$_2$][8] (0.2 g, 0.25 mmol) in water (30 cm^3) was added silver triflate (0.26 g, 1.0 mmol), and the mixture was stirred at 40 °C for 1 h. The resulting precipitate of silver chloride was removed by filtration. To the filtrate was added an aqueous solution (50 cm^3) of H_2put (0.076 g, 0.5 mmol) to give a yellow precipitate, which was dissolved again by adding ethanol (50 cm^3). The resulting solution was refluxed at 80 °C for 2 h and then evaporated to give a yellow powder. The yield was 45%. Anal. Calcd for [{Ir(Cp*)(Hput)}$_4$](CF$_3$SO$_3$)$_4$·4H$_2$O **2** ($C_{64}H_{80}F_{12}Ir_4N_{16}O_{16}S_8$): C, 29.76; H, 3.12; N, 8.68. Found: C, 29.84; H, 3.03; N, 8.68. UV−vis (CH$_3$CN) λ_{max}, nm (ϵ, dm^3 mol^{-1} cm^{-1}): 354 (37 900), 272 (30 500). ESI MS (*m*/*z* in CH$_3$CN): 956 ([4M − 4X − 2H]$^{2+}$), 1911 ([4M − 4X − 3H]$^+$).

[{Ru(Hput)(cymene)}$_4$](CF$_3$SO$_3$)$_4$ (3). To a suspension of [{RuCl$_2$(cymene)}$_2$][9] (0.2 g, 0.32 mmol) in water (30 cm^3) was added silver triflate (0.33 g, 1.3 mmol), and the mixture was stirred at 40 °C for 1 h. The resulting precipitate of silver chloride was removed by filtration, and an aqueous solution (50 cm^3) of H_2put (0.076 g, 0.5 mmol) was adjusted to ca. pH 7 by adding aqueous NaOH to the filtrate. After being refluxed at 80 °C for 2 h, the reaction solution was evaporated to give a yellow powder. The yield was 25%. Anal. Calcd for [{Ru(Hput)(cymene)}$_4$](CF$_3$SO$_3$)$_4$·8H$_2$O (**3**) ($C_{64}H_{84}F_{12}N_{16}O_{20}Ru_4S_8$): C, 33.62; H, 3.70; N, 9.80. Found: C, 33.75; H, 3.69; N, 10.15. UV−vis (CH$_3$CN) λ_{max}, nm (ϵ, dm^3 mol^{-1} cm^{-1}): 354 (35 100), 274 (29 500). ESI MS (*m*/*z* in CH$_3$CN): 387 ([4M − 4X]$^+$), 515.7 ([4M − 4X − H]$^{3+}$), 773 ([4M − 4X − 2H]$^{2+}$), 846 ([4M − 3X − H]$^{2+}$).

[{Rh(Cp*)(Haput)}$_2$](CF$_3$SO$_3$)$_2$ (4a) and [{Rh(Cp*)(Haput)}$_4$](CF$_3$SO$_3$)$_4$ (4b). This complex was prepared in the same manner as **1** using H_2aput but without aqueous NaOH. The yield of orange powder **4a** was 50%. Anal. Calcd for [{Rh(Cp*)(Haput)}$_2$](CF$_3$SO$_3$)$_2$·3H$_2$O (**4a**) ($C_{32}H_{44}F_6N_{10}O_9Rh_2S_4$): C, 33.11; H, 3.82; N, 12.07. Found: C, 32.80; H, 3.82; N, 12.10. UV−vis (CH$_3$CN) λ_{max}, nm (ϵ, dm^3 mol^{-1} cm^{-1}): 369 (11 600), 323 (16 300), 283 (22 700), 241 (53 500). ESI MS (*m*/*z* in CH$_3$OH): 404.4 ([2M − 2X]$^{2+}$), 807.9 ([2M − 2X − H]$^+$), 957.4 ([2M − X]$^+$). The orange crystals **4b** were obtained from the methanol/ether solution of **4a**.

[{Ir(Cp*)(Haput)}$_4$](CF$_3$SO$_3$)$_4$ (5). This complex was prepared in the same manner as **2** using H_2aput. The yield of yellow powder was 80%. Anal. Calcd for [{Ir(Cp*)(Haput)}$_4$](CF$_3$SO$_3$)$_4$·6H$_2$O (**5**) ($C_{64}H_{88}F_{12}Ir_4N_{20}O_{18}S_8$): C, 28.69; H, 3.31; N, 10.46. Found: C, 28.69; H, 3.35; N, 10.57. NMR (600 MHz, DMSO-d_6, 25 °C, TMS): δ_C = 164.67 (C6), 154.64 (C2 and C4), 151.21 (C8), 134.33 (C5), 88.86 (Cp*), 9.07 (Cp*). ESI MS (*m*/*z* in CH$_3$OH): 658.3 ([4M − 4X − H]$^{3+}$), 708.3 ([4M − 3X]$^{3+}$), 986.1 ([4M − 4X − 2H]$^{2+}$), 1062 ([4M − 3X − H]$^{2+}$), 1137 ([4M − 2X]$^{2+}$).

[{Ru(Haput)(cymene)}$_2$]$^{2+}$ (6a) and [{Ru(Haput)(cymene)}$_4$](CF$_3$SO$_3$)$_4$ (6b). This complex was prepared in the same manner as **3** using H_2aput. The ^{1}H NMR spectrum of the reaction solution showed the existence of two species, dominant (**6a**) and minor (**6b**). The subsequent crystallization process always increased the ratio of the latter species. Finally, the yellow solid **6b** was isolated as a single powder (40%). **6b**: Anal. Calcd for [{Ru(Haput)(cymene)}$_4$](CF$_3$SO$_3$)$_4$·6H$_2$O ($C_{64}H_{80}F_{12}N_{20}O_{18}Ru_4S_8$): C, 33.33; H, 3.50; N, 12.15. Found: C, 33.50; H, 3.58; N, 12.52. UV−vis (CH$_3$CN) λ_{max}, nm (ϵ, dm^3 mol^{-1} cm^{-1}): 355 (32 500). ESI MS (*m*/*z* in CH$_3$CN): 402 ([M − X]$^+$), 535.7 ([4M − 4X − H]$^{3+}$), 584.3 ([4M − 3X]$^{3+}$), 803 ([4M − 4X − 2H]$^{2+}$), 876 ([4M − 3X − H]$^{2+}$), 949 ([4M − 2X]$^{2+}$).

ESI Mass Spectral Measurements. ESI mass spectra were obtained by a sector-type mass spectrometer (JEOL-D300) connected with a laboratory-made ESI interface.[10] A sample solution was sprayed from the tip of a needle by applying a voltage 3.5 kV higher than that of a counter electrode. The distance between the needle and the counter electrode was 1 cm. The counter electrode consisted of a 12-cm-long stainless steel capillary tube (0.5 mm i.d.). A stream of heated N_2 gas (70 °C) was used to aid desolvation of sprayed charged droplets. The flow rate of the sample solution was 2 mL/min, and the corn voltage was 50 eV. The samples were dissolved in freshly distilled acetonitrile or methanol, and nothing was added to promote ionization. The concentrations of samples were kept at ca. 10^{-4} mol dm^{-3}.

X-ray Structure Determinations. A red block crystal (0.40 mm × 0.40 mm × 0.30 mm) of [{Rh(Cp*)(H$_{0.5}$put)}$_4$](CF$_3$SO$_3$)$_2$·2Et$_2$O·6H$_2$O **(1b)** and a yellow plate crystal (0.20 mm × 0.15 mm ×

(7) (a) Cusanelli, A.; Frey, U.; Richens, D. T.; Merbach, A. E. *J. Am. Chem. Soc*. **1996**, *118*, 5265−5271. (b) Cayemittes, S.; Poth, T.; Fernandez, M. J.; Lye, P. G.; Becker, M.; Elias, H.; Merbach, A. E. *Inorg. Chem*. **1999**, *38*, 4309−4316.
(8) White, C.; Yates, A.; Maitlis, P. M. *Inorg. Synth.* **1992**, *29*, 228−234.
(9) Bennett, M. A.; Huang, T.-N.; Matheson, T. W.; Smith, A. K. *Inorg. Synth*. **1982**, *21*, 74−78.
(10) Arakawa, R.; Tachiyashiki, S.; Matsuo, T. *Anal. Chem*. **1995**, *67*, 4133−4138.

Table 1. Crystallographic Data for $[\{Rh(Cp^*)(H_{0.5}put)\}_4](CF_3SO_3)_2 \cdot 2Et_2O \cdot 6H_2O$ (**1b**) and $[\{Ir(Cp^*)(Haput)\}_4](CF_3SO_3)_4 \cdot 6H_2O$ (**5**)

	1b	**5**
formula	$C_{70}H_{102}F_6N_{16}O_{14}Rh_4S_6$	$C_{64}H_{88}F_{12}Ir_4N_{20}O_{18}S_8$
fw	2109.65	2678.86
space group	$P4_2/n$ (No. 86)	$P2_1/n$ (No. 14)
cryst syst	tetragonal	monoclinic
a, Å	21.3823(3)	15.215(1)
b, Å		40.176(4)
c, Å	20.1766(3)	14.946(1)
β, deg		90.722(2)
V, Å^3	9224.8(2)	9135(1)
Z	4	4
ρ (calcd), g cm^{-3}	1.519	1.948
μ(Mo Kα), cm^{-1}	9.13	61.04
temp, K	296	296
R1[a]	0.047	0.085
wR2[a]	0.145	0.196

[a] Quantity minimized = wR2 = $[\sum w(F_o^2 - F_c^2)^2/\sum w(F_o^2)^2]^{1/2}$; R1 = $\sum||F_o| - |F_c||/\sum|F_o|$.

0.04 mm) of $[\{Ir(Cp^*)(Haput)\}_4](CF_3SO_3)_4 \cdot 6H_2O$ **(5)** were obtained from DMF/Et_2O and MeOH/Et_2O, respectively, at room temperature. Diffraction data were collected on a Rigaku RAXIS-RAPID imaging plate with graphite-monochromated Mo Kα radiation (λ = 0.71069 Å). Crystallographic data are listed Table 1. The structure was solved by direct methods. Some non-hydrogen atoms were refined anisotropically, while the rest were refined isotropically. Hydrogen atoms were included but not refined for both complexes. The final cycle of full-matrix least squares was based on 6669 observed reflections ($I > 2\sigma I$) and 424 variable parameters for **1b** and on 11 418 reflections and 788 parameters for **5**. 10 583 reflections for **1b** and 18 456 for **5** were collected. Refinement was carried out on F. The final values of R1 and wR2 were 0.047 and 0.145 for **1b** and 0.085 and 0.196 for **5**. All calculations were performed using the teXsan[11] crystallographic software package of Molecular Structure Corporation.

Measurements. UV−vis absorption spectra were measured with a Hitachi 330 spectrophotometer, CD spectra were measured with a JASCO J-500 spectrophotometer, and ^{1}H and ^{13}C NMR spectra were measured with a JEOL JNM-GSX-270 and VARIAN UNITY plus-600 NMR spectrometer in $(CD_3)_2SO$ at 30 °C. X-ray crystal analysis was made at the X-ray diffraction service of the Department of Chemistry.

Results and Discussion

Preparations of Complexes and Their ESI Mass Spectra. The reaction of $[M(Cp^*)(H_2O)_3]^{2+}$ (M = Rh^{III} and Ir^{III}) and H_2put will produce a mononuclear species $[M(Cp^*)(Hput\text{-}N,S)H_2O]^+$ shown first in Scheme 1. The subsequent self-assembly reaction between the mononuclear species will lead to the formation of cyclic polynuclear complexes $[\{M(Cp^*)(Hput\text{-}N,S,N')\}_n]^{n+}$. This synthetic strategy has been effectively realized in all the present systems.[12]

In the case of the H_2put ligand, a single species was found both in the reaction solutions and in the isolated complexes **1a**−**3** for all metal systems. The complexes **1a**−**3** in Table

Scheme 1

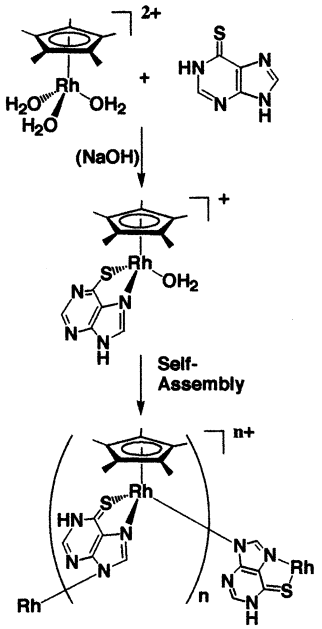

2 showed one very similar set of ^{1}H NMR signals. The H^8 signal tends to become broader than the H^2 signal. These results suggest that they have the same structure. Complex **1a** showed four dominant ESI mass spectral peaks at m/z = 519.1, 777.8, 852.7, and 927.3. They all correspond to the tetranuclear ions of $[4M - 4X - H]^{3+}$, $[4M - 4X - 2H]^{2+}$, $[4M - 3X - H]^{2+}$, and $[4M - 2X]^{2+}$, respectively, where M and X represent the mononuclear unit complex and $CF_3SO_3^-$, respectively. Similarly, complex **2** showed two peaks at m/z = 956 ($[4M - 4X - 2H]^{2+}$) and 1911 ($[4M - 4X - 3H]^+$), and complex **3** showed four peaks at m/z = 387 ($[4M - 4X]^+$), 515.7 ($[4M - 4X - H]^{3+}$), 773 ($[4M - 4X - 2H]^{2+}$), and 846 ($[4M - 3X - H]^{2+}$). These results confirm that complexes **1a**−**3** are all cyclic tetranuclear species.

In the Ir^{III}-H_2aput system, a single species was found both in the reaction solution and in the isolated complex **5**. However, two species were found in the Rh-H_2aput and Ru-H_2aput systems. Complex **4a** was dominant in the reaction solution despite the presence or absence of alkali and was isolated as a pure powder. Interestingly, recrystallization of **4a** from the methanol/ether solution gave the different species **4b**, which corresponds to a minor component in the reaction solution. The situation in Ru-H_2aput is quite analogous to the Rh^{III} case. The dominant species **6a** in the reaction solution turned finally into **6b** through the crystallization process. This means that the presence of equilibrium in solution and the prolonged crystallization resulted in another species, **4b** or **6b**. The ^{1}H NMR spectra of **4b**, **5**, and **6b** are very similar to each other, but those of **4a** and **6a** are different from the others. Complex **5** showed five dominant ESI mass spectral peaks at m/z = 658.3 ($[4M - 4X - H]^{3+}$), 708.3 ($[4M - 3X]^{3+}$), 986.1 ($[4M - 4X - 2H]^{2+}$), 1062 ($[4M - 3X - H]^{2+}$), and 1137 ($[4M - 2X]^{2+}$). Similarly, complex **6b** showed five peaks at m/z = 535.7 ($[4M - 4X - H]^{3+}$), 584.3 ($[4M - 3X]^{3+}$), 803 ($[4M - 4X - 2H]^{2+}$), 876 ($[4M - 3X - H]^{2+}$), and 949 ($[4M - 2X]^{2+}$). They all correspond

(11) *TEXSAN-TEXRAY Structure Analysis Package*; Molecular Structure Corp.: Houston, TX, 1985 and 1992.
(12) (a) Smith, D. P.; Bruce, E.; Morales, B.; Olmstead, M. M.; Maestre, M. F.; Fish, R. H. *J. Am. Chem. Soc*. **1992**, *114*, 10647−10649. (b) Smith, D. P.; Kohen, E.; Maestre, M. F.; Fish, R. H. *Inorg. Chem.* **1993**, *32*, 4119−4122. (c) Chen, H.; Ogo, S.; Fish, R. H. *J. Am. Chem. Soc*. **1996**, *118*, 4993−5001.

Table 2. Proton NMR Spectral Data (δ)[a] of the Prepared Complexes

	^{1}H MMR			
	NH	H^2/N^2H_2	H^8	Cp*/cymene
$[\{Rh(Cp^*)(Hput)\}_4]^{4+}$ (**1a**)		8.208(s, 1H)	7.939(s, 1H)	1.637(s, 15H)
$[\{Ir(Cp^*)(Hput)\}_4]^{4+}$ (**2**)		8.292(s, 1H)	8.043(s, 1H)	1.677(s, 15H)
$[\{Ru(Hput)(cymene)\}_4]^{4+}$ (**3**)		8.235(s, 1H)	8.312(s, 1H)	6.572(d, 1H) 6.084(d, 1H) 5.847(d, 1H) 5.722(d, 1H) 2.270(qui, 1H) 1.571(s, 3H) 1.021(d, 3H) 0.735(d, 3H)
$[\{Rh(Cp^*)(Haput)\}_2]^{2+}$ (**4a**)	13.379(s, 1H)	6.549(s, 2H)	8.601(s, 1H)	1.759(s, 15H)
$[\{Rh(Cp^*)(Haput)\}_4]^{4+}$ (**4b**)	12.771(s, 1H)	6.971(s, 2H)	7.695(s, 1H)	1.631(s, 15H)
$[\{Ir(Cp^*)(Haput)\}_4]^{4+}$ (**5**)	13.012(s, 1H)	7.096(s, 2H)	7.729(s, 1H)	1.669(s, 15H)
$[\{Ru(Haput)(cymene)\}_2]^{2+}$ (**6a**)	13.450(s, 1H)	6.629(s, 2H)	8.487(s, 1H)	6.455(d, 1H) 6.261(d, 1H) 6.070(d, 1H) 5.855(d, 1H) 2.802(m, 1H) 2.208(s, 3H) 1.267(d, 3H) 1.033(d, 3H)
$[\{Ru(Haput)(cymene)\}_4]^{4+}$ (**6b**)	12.842(s, 1H)	6.897(s, 2H)	7.858(s, 1H)	6.243(t, 2H) 5.637(d, 1H) 5.481(d, 1H) 2.223(t, 1H) 1.794(s, 3H) 1.160(d, 3H) 0.880(d, 3H)

[a] Downfield relative to $SiMe_4$ in $(CD_3)_2SO$.

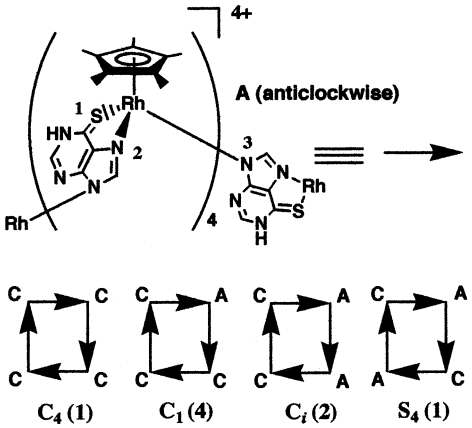

Figure 1. Four possible isomers of a cyclic tetramer. The characters *C* (clockwise) and *A* (anticlockwise) denote the chiralities of the unit complex. Each isomer is denoted by its complex symmetry, and the number in parentheses shows the expected NMR sets.

to the tetranuclear ions and, hence, complexes **5** and **6b** are assigned to cyclic tetranuclear species. On the other hand, complex **4a** showed three ESI mass spectral peaks at m/z = 404.4 ($[2M - 2X]^{2+}$), 807.9 ($[2M - 2X - H]^+$), and 957.4 ($[2M - X]^+$), which correspond to dinuclear compositions. Thus, complex **4a** was assigned to a dimer, and **4b** was assigned to a tetramer on the basis of X-ray crystal structure analyses described below.

Geometrical Isomerism. Since all complexes except **4a** and **6a** belong to tetranuclear species, we have to consider the geometrical isomerism of the cyclic tetramer. The unit complex that indicates each component Rh monomer should be expressed as an arrow because it is unsymmetrical and has a head and a tail as shown in Figure 1. For example, the head denotes the N,S-chelating moiety, and the tail signifies the moiety bridging to another metal ion. The arrows must be arrayed in the same direction to form a circle. It should be noted that the structures where two arrows converge on one metal unit never become cyclic. Each unit complex has chirality *C* (clockwise) or *A* (anticlockwise)[13] because it belongs to a $[M(A_3)(BC)D]$ type.[14]

(13) Leigh, G. J., Ed. *Nomenclature of Inorganic Chemistry, Recommendation 1990*; Blackwell: Oxford, UK, 1990.
(14) Yamanari, K.; Hidaka, J.; Shimura, Y. *Bull. Chem. Soc. Jpn.* **1975**, *48*, 1653−1654.

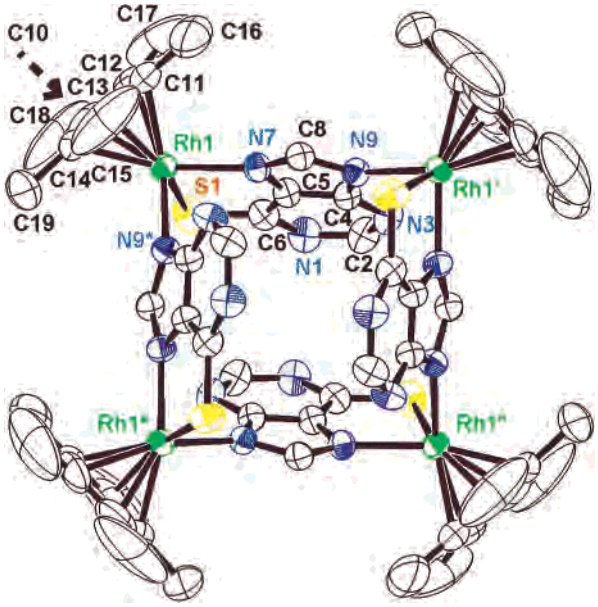

Figure 2. X-ray crystal structure of the cation of $[\{Rh(Cp^*)(H_{0.5}put)\}_4](CF_3SO_3)_2 \cdot 2Et_2O \cdot 6H_2O$ (**1b**).

There are four isomers for the cyclic tetranuclear structure. The symmetries of the isomers are C_4(*CCCC* + *AAAA*), C_1(*CCCA* + *AAAC*), C_i(*CCAA*), and S_4(*CACA*). The numbers in parentheses indicate the expected NMR set. For example, the three *C* sites in the C_1 isomer are chemically different because both the head and the tail at each site are different from those of the others, and hence, four NMR sets are expected for this isomer. The latter two isomers are achiral.

The present Hput and Haput complexes except **4a** and **6a** have the cyclic tetranuclear structure as determined by ESI mass spectra. All these tetramers showed one set of ^{1}H NMR spectra in Table 2 and hence are concluded to be the C_4 or S_4 isomer. Three S_4 structures for **1b**, **4b**, and **5** are confirmed by X-ray crystal structure analyses described below.

Crystal Structure of $[\{Rh(Cp^*)(H_{0.5}put)\}_4](CF_3SO_3)_2$. Figure 2 shows the view of the cation and the numbering scheme in $[\{Rh(Cp^*)(H_{0.5}put)\}_4](CF_3SO_3)_2 \cdot 2Et_2O \cdot 6H_2O$ (**1b**). This crystal was produced from $[\{Rh(Cp^*)(Hput)\}_4](CF_3SO_3)_4$ (**1a**) by spontaneous deprotonation during recrystallization in DMF/ether, and hence, complex **1b** does not have

Table 3. Selected Bond Distances (Å) and Bond Angles (deg) for [{Rh(Cp*)($H_{0.5}$put)}$_4$](CF_3SO_3)$_2$·2Et_2O·6H_2O (**1b**)

molecule 1		molecule 2	
Bond Distances			
Rh(1)−S(1)	2.450(1)	Rh(2)−S(2)	2.442(1)
Rh(1)−N(7)	2.131(3)	Rh(2)−N(27)	2.128(3)
Rh(1)−N(9)	2.099(3)	Rh(2)−N(29)	2.097(3)
Rh(1)−C(10)	2.174(6)	Rh(2)−C(30)	2.163(7)
Rh(1)−C(11)	2.165(6)	Rh(2)−C(31)	2.163(7)
Rh(1)−C(12)	2.147(6)	Rh(2)−C(32)	2.130(6)
Rh(1)−C(13)	2.152(6)	Rh(2)−C(33)	2.151(7)
Rh(1)−C(14)	2.143(6)	Rh(2)−C(34)	2.126(6)
S(1)−C(6)	1.711(4)	S(2)−C(26)	1.720(4)
N(1)−C(2)	1.362(6)	N(21)−C(22)	1.362(6)
N(1)−C(6)	1.353(6)	N(21)−C(26)	1.358(5)
N(3)−C(2)	1.325(6)	N(23)−C(22)	1.316(6)
N(3)−C(4)	1.355(5)	N(23)−C(24)	1.361(5)
N(7)−C(5)	1.361(5)	N(27)−C(25)	1.363(5)
N(7)−C(8)	1.339(5)	N(27)−C(28)	1.340(5)
N(9)−C(4)	1.380(5)	N(29)−C(24)	1.376(5)
N(9)−C(8)	1.362(5)	N(29)−C(28)	1.360(5)
C(4)−C(5)	1.378(6)	C(24)−C(25)	1.382(6)
C(5)−C(6)	1.387(6)	C(25)−C(26)	1.369(6)
Bond Angles			
S(1)−Rh(1)−N(7)	84.08(9)	S(2)−Rh(2)−N(27)	84.06(9)
S(1)−Rh(1)−N(9)	91.46(10)	S(2)−Rh(2)−N(29)	91.64(10)
N(7)−Rh(1)−N(9)	84.3(1)	N(27)−Rh(2)−N(29)	84.5(1)
Rh(1)−S(1)−C(6)	96.9(1)	Rh(2)−S(2)−C(26)	96.7(1)
C(2)−N(1)−C(6)	120.0(4)	C(22)−N(21)−C(26)	119.4(4)
C(2)−N(3)−C(4)	112.2(4)	C(22)−N(23)−C(24)	112.0(4)
Rh(1)−N(7)−C(5)	112.2(3)	Rh(2)−N(27)−C(25)	112.3(3)
C(5)−N(7)−C(8)	103.9(3)	C(25)−N(27)−C(28)	103.8(3)
Rh(1)−N(9)−C(4)	124.3(3)	Rh(2)−N(29)−C(24)	124.0(3)
Rh(1)−N(9)−C(8)	131.6(3)	Rh(2)−N(29)−C(28)	131.4(3)
C(4)−N(9)−C(8)	104.0(3)	C(24)−N(29)−C(28)	104.4(3)
N(1)−C(2)−N(3)	127.8(4)	N(21)−C(22)−N(23)	128.1(4)
N(3)−C(4)−C(5)	123.7(4)	N(23)−C(24)−C(25)	123.4(4)
N(9)−C(4)−C(5)	107.6(3)	N(29)−C(24)−C(25)	107.3(3)
N(7)−C(5)−C(4)	110.3(3)	N(27)−C(25)−C(24)	110.3(3)
C(4)−C(5)−C(6)	121.4(4)	C(24)−C(25)−C(26)	121.4(4)
S(1)−C(6)−C(5)	118.4(3)	S(2)−C(26)−C(25)	118.6(3)
N(1)−C(6)−C(5)	114.9(4)	N(21)−C(26)−C(25)	115.4(4)
N(7)−C(8)−N(9)	114.3(4)	N(27)−C(28)−N(29)	114.1(4)

a 4+ but a 2+ charge. The crystallographic data are shown in Table 1, and selected bond distances and angles are listed in Table 3. Complex **1b** has a tetranuclear structure, and two independent molecules Rh(1) and Rh(2)[15] exist in the unit cell. They are similar to each other, and Figure 2 shows the only Rh(1) structure. Four Rh^{III} ions of each molecule are crystallographically equivalent, and **1b** has an alternate chirality array of *CACA*, adopting S_4 symmetry. The Rh···Rh distance is 6.4262(4) Å for Rh(1) and 6.4179(4) Å for Rh(2), which are longer than the Co···Co distance of 6.118 Å in [{Co(Hput)(tacn)}$_4$](CF_3SO_3)$_4$.[4] All Hput ligands adopt a μ-1κN^9:2$\kappa^2 S^6$,N^7 bridging mode: they coordinate to one Rh^{III} ion in a bidentate manner via the S^6 and N(7) donors, which form a five-membered chelate ring and bridge to another Rh^{III} ion through the N(9) donor, respectively. The orientations of the four $H_{0.5}$put ligands are alternately up and down. These four ligands form a central square cavity as shown in Figure 3. The cavity becomes narrow at both sides because of $\pi-\pi$ stacking interactions between the

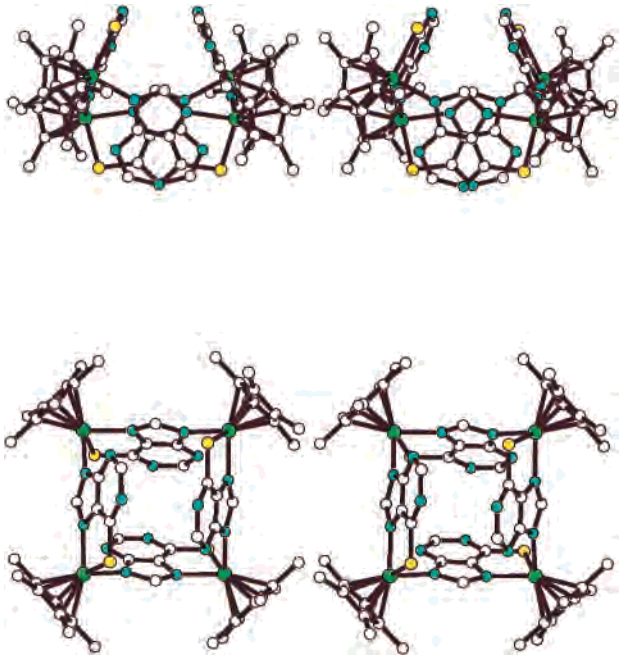

Figure 3. Side (above) and top (below) stereoviews of the cation of **1b**.

opposite two $H_{0.5}$put ligands: the distance N(1)···N(1)″ and N(1)···C(2)″ are 3.216(8) and 3.578(6) Å, respectively.

Particularly interesting is the stacking pattern in the solid state. The bottom view of Figure 4 shows the packing of cationic tetramers in the *ab* plane. These tetramers are stacked up along the *c* axis, resulting in an infinite channel-like cavity (top view). The order of the Rh(1) and Rh(2) molecules is alternate. The repeating unit distance between each stacked cationic tetramer is 10.1 Å (= *c*/2). The driving force of this stacking is due to double hydrogen bonds [N(1)−H in Rh(1)···N(21) in Rh(2) = 2.752(4) Å] at both sides of the cavity.

It is quite intriguing that the infinite structure **1b** was spontaneously formed from **1a** in DMF/ether solution. Complex **1a** showed an ESI mass peak at m/z = 777.8 assignable to $[4M - 4X - 2H]^{2+}$. Similarly, complexes **2** and **3** showed the corresponding peaks at m/z = 956 ($[4M - 4X - 2H]^{2+}$) and 773 ($[4M - 4X - 2H]^{2+}$), respectively. These results clearly reveal the existence of 2+ complex cations in **2** and **3**, and complexes **2** and **3** also have the same cyclic S_4 structure as **1b**. Thus, every tetramer tends to stack up along one axis to form an infinite channel-like cavity through intermolecular double hydrogen bonds in the Hput systems. Although there are some channel-like packing structures without special interactions,[16] the present stacking of cationic cyclic tetramers by double hydrogen bonds is quite novel.

In the previous Co^{III} system, four intramolecular hydrogen bonds between N(3) and H−N(tacn) were found in S_4-[{Co(Hput)(tacn)}$_4$]$^{4+}$ and contribute to the stability of the cyclic tetramer of *CACA*. Such intramolecular hydrogen bonds may

(15) The numbering scheme of Rh(2) is as follows: Rh(1) and S(1) in Figure 2 become Rh(2) and S(2), respectively, and the number 20 is added to each atom number for the remaining nitrogen and carbon atoms.

(16) (a) Stang, P. J.; Cao, D. H.; Saito, S.; Arif, A. M. *J. Am. Chem. Soc.* **1995**, *117*, 6273−6283. (b) Stang, P. J.; Chen, K.; Arif, A. M. *J. Am. Chem. Soc.* **1995**, *117*, 8793−8797. (c) Cotton, F. A.; Daniels, L. M.; Lin, C.; Murillo, C. A. *J. Am. Chem. Soc.* **1999**, *121*, 4538−4539.

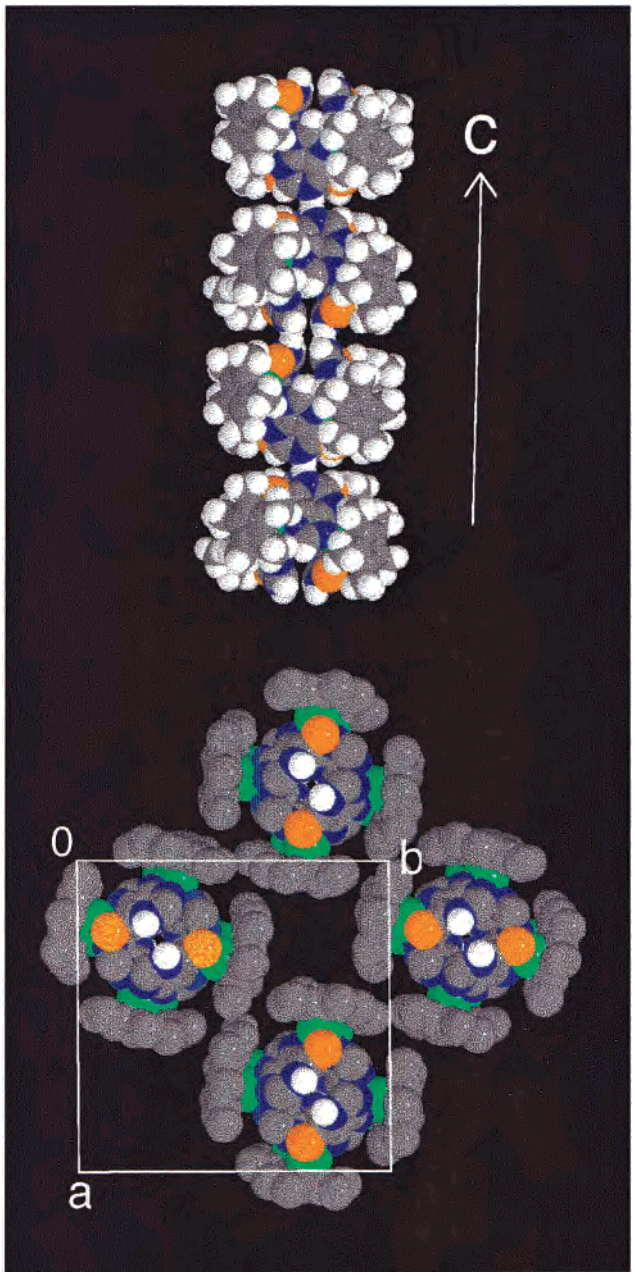

Figure 4. Space-filling structures of an infinite channel-like stacking of the cyclic tetramers in the *ab* plane (bottom) and along the *c* axis (top) in **1b**.

promote the facile formation of a *CA* chirality pair in solution. In fact, a rare cyclic C_1 trimer $[\{Co(Hput)(tacn)\}_3]^{3+}$ was also formed in the Co^{III} system because either attack of *C* or *A* to a *CA* pair results in the formation of the C_1 trimer of *CCA* or *ACA*, respectively. In the present system without intramolecular interactions, the cyclic S_4 tetramer was formed as a single species and could be stacked up along the *c* axis through the double intermolecular hydrogen bonds instead.

Crystal Structure of $[\{Ir(Cp^*)(Haput)\}_4](CF_3SO_3)_4$. Figure 5 shows the view of the cation and the numbering scheme in $[\{Ir(Cp^*)(Haput)\}_4](CF_3SO_3)_4\cdot 6H_2O$ (**5**). The crystallographic data are shown in Table 1, and selected bond distances and angles are listed in Table 4. Complex **5** also has a cyclic tetranuclear structure, although four Ir^{III} ions are crystallographically independent. Complex **5** adopts S_4

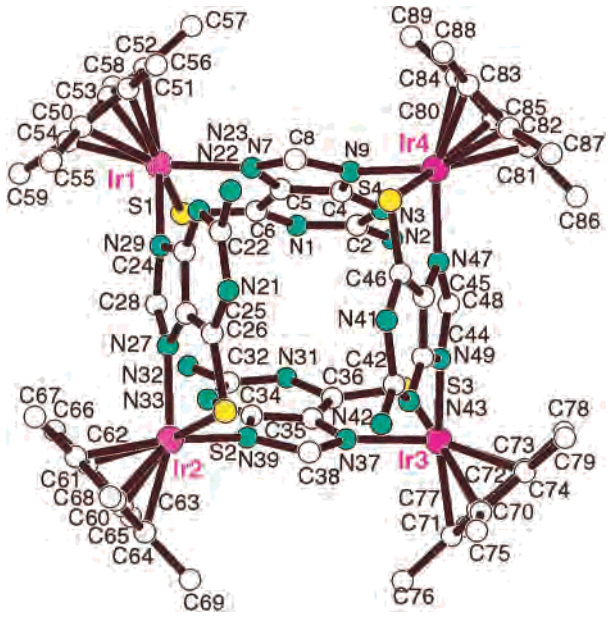

Figure 5. X-ray crystal structure of the cation in $[\{Ir(Cp^*)(Haput)\}_4](CF_3SO_3)_4\cdot 6H_2O$ (**5**).

Table 4. Selected Bond Distances (Å) and Bond Angles (deg) for $[\{Ir(Cp^*)(Haput)\}_4](CF_3SO_3)_4\cdot 6H_2O$ **5**

Bond Distances			
Ir(1)−S(1)	2.432(4)	Ir(3)−S(3)	2.426(4)
Ir(1)−N(7)	2.11(1)	Ir(3)−N(37)	2.14(1)
Ir(1)−N(29)	2.10(1)	Ir(3)−N(49)	2.14(1)
Ir(1)−C(50)	2.22(2)	Ir(3)−C(70)	2.16(2)
Ir(1)−C(51)	2.23(1)	Ir(3)−C(71)	2.18(2)
Ir(1)−C(52)	2.18(1)	Ir(3)−C(72)	2.16(1)
Ir(1)−C(53)	2.19(1)	Ir(3)−C(73)	2.20(2)
Ir(1)−C(54)	2.12(2)	Ir(3)−C(74)	2.18(1)
Ir(2)−S(2)	2.418(4)	Ir(4)−S(4)	2.435(4)
Ir(2)−N(27)	2.12(1)	Ir(4)−N(9)	2.13(1)
Ir(2)−N(39)	2.06(1)	Ir(4)−N(47)	2.11(1)
Ir(2)−C(60)	2.16(2)	Ir(4)−C(80)	2.14(2)
Ir(2)−C(61)	2.11(3)	Ir(4)−C(81)	2.13(1)
Ir(2)−C(62)	2.17(3)	Ir(4)−C(82)	2.07(2)
Ir(2)−C(63)	2.10(2)	Ir(4)−C(83)	2.14(2)
Ir(2)−C(64)	2.13(2)	Ir(4)−C(84)	2.16(2)
S(1)−C(6)	1.69(1)	S(3)−C(36)	1.69(2)
S(2)−C(26)	1.75(1)	S(4)−C(46)	1.65(1)
Bond Angles			
S(1)−Ir(1)−N(7)	84.1(3)	S(3)−Ir(3)−N(37)	82.9(3)
S(1)−Ir(1)−N(29)	91.8(3)	S(3)−Ir(3)−N(49)	91.1(3)
N(7)−Ir(1)−N(29)	83.0(5)	N(37)−Ir(3)−N(49)	83.3(5)
S(2)−Ir(2)−N(27)	84.0(3)	S(4)−Ir(4)−N(9)	90.6(3)
S(2)−Ir(2)−N(39)	91.1(4)	S(4)−Ir(4)−N(47)	82.5(3)
N(27)−Ir(2)−N(39)	84.7(4)	N(9)−Ir(4)−N(47)	85.7(5)
Ir(4)−N(9)−C(4)	124(1)	Ir(2)−N(39)−C(34)	125(1)
Ir(4)−N(9)−C(8)	127(1)	Ir(2)−N(39)−C(38)	131.0(9)
Ir(1)−N(29)−C(24)	122.5(9)	Ir(3)−N(49)−C(44)	120.7(10)
Ir(1)−N(29)−C(28)	130.9(10)	Ir(3)−N(49)−C(48)	131(1)

symmetry with an alternate chirality array of *CACA*, and all Haput ligands take a μ-1κN^9:2$\kappa^2 S^6$,N^7 bridging mode. The orientations of the four Haput ligands are alternately up and down.

The side view of Figure 6 shows a central square cavity formed by four Haput ligands. The central cavity size (Ir···Ir = av 6.409 Å) is a little smaller than that of **1b**. The cavity becomes narrow on both sides because of $\pi-\pi$ stacking interactions between the opposite two Haput ligands: the distances N(1)···N(31) and N(21)···N(41) are 3.49(2) and 3.52(2) Å, respectively. The most striking

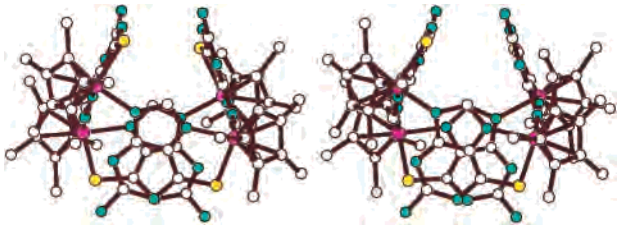

Figure 6. Side stereoview of the cation of **5**.

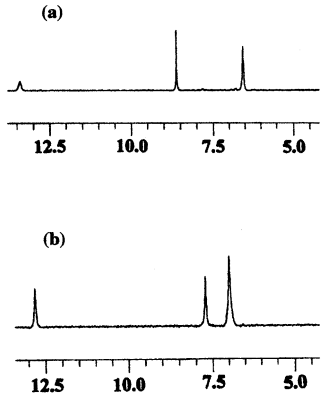

Figure 7. Proton NMR spectra (in $(CD_3)_2SO$) of two species [**4a** (a) and **4b** (b)] in the Rh-H_2aput system.

difference, however, is the absence of the stacking structure: all N(1) sites of the Haput ligands in **5** are fully protonated and cannot participate in intermolecular hydrogen bonds. In addition, model considerations showed that the stacking structure in **1b** becomes impossible for **5** because of the intermolecular steric repulsion between the 2-amino groups. Such a situation is well-understandable in Figure 6.

Characterization of Two Species in Rh- and Ru-H_2aput Systems. Two species **4a** and **4b** were obtained in the Rh-H_2aput system. These ^{1}H NMR spectra are quite different from each other in Figure 7. The ^{1}H NMR spectral pattern of **4b** is very similar to those of tetramers **5** and **6**. The crystal structure determination of **4b** was made, and it turned out that **4b** has the same S_4 structure as **5**, although the crystal data were of considerably low quality.[17]

ESI mass spectra showed that complex **4a** has a dimeric structure. When the ligand adopts a μ-1κN^9:2$\kappa^2 S^6$,N^7 bridging mode as found in **5**, the dimeric structure could not be formed. Recently, we have revealed that the μ-1κS^6:2$\kappa^2 S^6$,N^7 coordination mode is the most adequate for the dimeric structure: two geometrical isomers, syn and anti, are possible as shown in Figure 8.[18] In the syn dimer, the H^8 proton is located just above the six-membered ring of another purine, and hence, an upfield shift is expected. The H^8 signal of **4a**, however, appears at δ 8.601, whose value is exceptionally lower than those of **4b**, **5**, and **6**. Thus, complex **4a** is

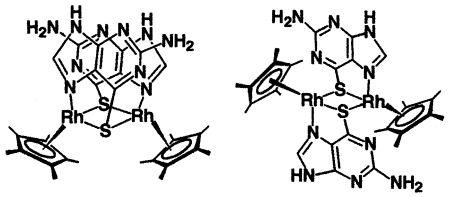

Figure 8. Proposed syn- and anti-dimeric structures.

tentatively assigned not to syn- but to anti-dimeric structure. A similar anti structure was found in [{Rh(Cp*)(mpol)}$_2$] [mpol = 2-sulfanyl-3-pyridinolate(2−)] where mpol adops a five-membered chelating mode of μ-1κS:2$\kappa^2 S,O$.[18]

In the Ru-H_2aput system, two species **6a** and **6b** were identified by ^{1}H NMR spectroscopy (Table 1). ESI mass spectra showed that complex **6b** has a tetrameric structure. On the other hand, the observed chemical shifts of N^2H_2 and H^8 for **6a** are quite different from those for **6b** but are very similar to those for the **4a**-dimeric structure. Hence, we tentatively concluded that **6a** has the same anti-dimeric structure as **4a**.

Conclusion

The present study reports six new cyclic tetramers with Hput or Haput, and we concluded that they all adopt the S_4 structure. Eight crystal structures have been reported so far for the cyclic tetramers with half-sandwich types: [{RuCl(Hade)(η^6-C_6H_6)}$_4$]Cl$_4$,[19] [{RuCl(N^6-methyl-ade)(η^6-C_6H_6)}$_4$],[19] [{Ru(ade)(cymene)}$_4$]$(CF_3SO_3)_4$,[5] [{Ir(Cp*)(ade)}$_4$]$(CF_3SO_3)_4$,[6] [{Co(Hput)(tacn)}$_4$]$(CF_3SO_3)_4$,[4] [{Co(Haput)(tacn)}$_4$]$(CF_3SO_3)_4$,[4] [{Ir(Cp*)(hypoxanthinato)(H_2O)}$_4$]$(CF_3SO_3)_4$,[6] and [{Ir(Cp*)(guaninato)(H_2O)}$_4$]$(CF_3SO_3)_4$.[6] Interestingly, all these eight tetramers adopt the S_4 structure. Although the S_4 structures in the Co-tacn system are stabilized by four intramolecular hydrogen bonds, the above results suggest that such interactions are not necessarily crucial. Thus, three isomers, C_4(*CCCC* + *AAAA*), C_1(*CCCA* + *AAAC*), and C_i(*CCAA*) in Figure 1, have never been found in any metal systems. The S_4 structure seems to have special stability in the cyclic tetramers because it gives an alternate chirality array of *CACA*, and the orientations of the four bridging ligands are alternately up and down to be able to avoid the steric repulsion.

In conclusion, three congeners (Hput, Haput, and ade) adopt similar coordination modes and lead to the same self-assembled architectures, that is, cyclic S_4 tetranuclear structures. We have further realized a possibility that the intermolecular hydrogen bonds can stack these cyclic tetramers into the infinite channel-like solid structure in the Hput system.

Supporting Information Available: X-ray crystallographic files in CIF format. This material is available free of charge via the Internet at http://pubs.acs.org.

IC020449O

(17) The crystal data for **4b** were very similar to those for **5**, and the structure was concluded to belong to the S_4 isomer, although it was solved only partially. Crystal data: monoclinic, space group $P2_1/n$ (no. 14), a = 15.156(6) Å, b = 39.80(3) Å, c = 15.104(9) Å, β = 90.00(2)°, V = 9111(9) Å^3, Z = 4.

(18) Yamanari, K.; Fukuda, I.; Yamamoto, S.; Kushi, Y.; Fuyuhiro, A.; Kubota, N.; Fukuo, T.; Arakawa, R. *J. Chem. Soc., Dalton Trans.* **2000**, 2131−2136.

(19) Sheldrick, W. S.; Hagen-Eckhard, H. S.; Heeb, S. *Inorg. Chim. Acta* **1993**, *206*, 15−21.